

Search for Signatures of Dark Matter Annihilation in the Galactic Center with HAWC

R. Alfaro,¹ C. Alvarez,² A. Andrés,³ E. Anita-Rangel,³ M. Araya,⁴ J.C. Arteaga-Velázquez,⁵ D. Avila Rojas,³ H.A. Ayala Solares,⁶ R. Babu,⁷ P. Bangale,⁶ A. Bernal,³ K.S. Caballero-Mora,² T. Capistrán,⁸ A. Carramiñana,⁹ F. Carreón,³ S. Casanova,¹⁰ A.L. Colmenero-Cesar,⁵ U. Cotti,⁵ J. Cotzomi,¹¹ S. Coutiño de León,¹² E. De la Fuente,¹³ D. Depaoli,¹⁴ P. Desiati,¹⁵ N. Di Lalla,¹⁶ R. Diaz Hernandez,⁹ B.L. Dingus,¹⁷ M.A. DuVernois,¹⁵ J.C. Díaz-Vélez,¹⁵ K. Engel,¹⁸ T. Ergin,⁷ C. Espinoza,¹ K. Fang,¹⁵ N. Fraija,³ S. Fraija,³ J.A. García-González,¹⁹ F. Garfias,³ N. Ghosh,²⁰ H. Goksu,¹⁴ A. Gonzalez Muñoz,¹ M.M. González,³ J.A. González,⁵ J.A. Goodman,¹⁸ S. Groetsch,²⁰ J. Gyeong,^{21, 22} J.P. Harding,¹⁷ S. Hernández-Cadena,²³ I. Herzog,⁷ J. Hinton,¹⁴ D. Huang,¹⁸ F. Hueyotl-Zahuantitla,² P. Hüntemeyer,²⁰ A. Iriarte,³ S. Kaufmann,²⁴ D. Kieda,²⁵ A. Lara,²⁶ K. Leavitt,²⁰ W.H. Lee,³ J. Lee,²⁷ H. León Vargas,¹ J.T. Linnemann,⁷ A.L. Longinotti,³ G. Luis-Raya,²⁴ K. Malone,¹⁷ O. Martinez,¹¹ J. Martínez-Castro,²⁸ H. Martínez-Huerta,²⁹ J.A. Matthews,³⁰ J. McEnergy,³¹ P. Miranda-Romagnoli,³² P.E. Mirón-Enriquez,³ J.A. Montes,³ J.A. Morales-Soto,⁵ E. Moreno,¹¹ M. Mostafá,⁶ M. Najafi,²⁰ A. Nayerhoda,¹⁰ L. Nellen,³³ M.U. Nisa,⁷ R. Noriega-Papaqui,³² N. Omodei,¹⁶ M. Osorio-Archila,³ E. Ponce,¹¹ Y. Pérez Araujo,¹ E.G. Pérez-Pérez,²⁴ C.D. Rho,²² A. Rodriguez Parra,⁵ D. Rosa-González,⁹ M. Roth,¹⁷ H. Salazar,¹¹ D. Salazar-Gallegos,⁷ A. Sandoval,¹ M. Schneider,¹⁸ J. Serna-Franco,¹ A.J. Smith,¹⁸ Y. Son,²⁷ R.W. Springer,²⁵ O. Tibolla,²⁴ K. Tollefson,⁷ I. Torres,⁹ R. Torres-Escobedo,²³ R. Turner,²⁰ F. Ureña-Mena,⁹ E. Varela,¹¹ L. Villaseñor,¹¹ X. Wang,³⁴ Z. Wang,³⁴ I.J. Watson,²⁷ H. Wu,¹⁵ S. Yu,³⁵ S. Yun-Cárcamo,¹⁸ H. Zhou,²³ and C. de León⁵

(HAWC Collaboration)

¹*Instituto de Física, Universidad Nacional Autónoma de México, Ciudad de Mexico, Mexico*

²*Universidad Autónoma de Chiapas, Tuxtla Gutiérrez, Chiapas, México*

³*Instituto de Astronomía, Universidad Nacional Autónoma de México, Ciudad de Mexico, Mexico*

⁴*Universidad de Costa Rica, San José 2060, Costa Rica*

⁵*Universidad Michoacana de San Nicolás de Hidalgo, Morelia, Mexico*

⁶*Temple University, Department of Physics, 1925 N. 12th Street, Philadelphia, PA 19122, USA*

⁷*Department of Physics and Astronomy, Michigan State University, East Lansing, MI, USA*

⁸*Università degli Studi di Torino, I-10125 Torino, Italy*

⁹*Instituto Nacional de Astrofísica, Óptica y Electrónica, Puebla, Mexico*

¹⁰*Institute of Nuclear Physics Polish Academy of Sciences, PL-31342 IFJ-PAN, Krakow, Poland*

¹¹*Facultad de Ciencias Físico Matemáticas, Benemérita Universidad Autónoma de Puebla, Puebla, Mexico*

¹²*Instituto de Física Corpuscular, CSIC, Universitat de València, E-46980, Paterna, Valencia, Spain*

¹³*Departamento de Física, Centro Universitario de Ciencias Exactas Ingenierías,*

Universidad de Guadalajara, Guadalajara, Mexico

¹⁴*Max-Planck Institute for Nuclear Physics, 69117 Heidelberg, Germany*

¹⁵*Dept. of Physics and Wisconsin IceCube Particle Astrophysics Center,
University of Wisconsin—Madison, Madison, WI, USA*

¹⁶*Department of Physics, Stanford University: Stanford, CA 94305-4060, USA*

¹⁷*Los Alamos National Laboratory, Los Alamos, NM, USA*

¹⁸*Department of Physics, University of Maryland, College Park, MD, USA*

¹⁹*Tecnológico de Monterrey, Escuela de Ingeniería y Ciencias,*

Ave. Eugenio Garza Sada 2501, Monterrey, N.L., Mexico, 64849

²⁰*Department of Physics, Michigan Technological University, Houghton, MI, USA*

²¹*C.D. Rho*

²²*Department of Physics, Sungkyunkwan University, Suwon 16419, South Korea*

²³*Tsung-Dao Lee Institute & School of Physics and Astronomy,
Shanghai Jiao Tong University, 800 Dongchuan Rd, Shanghai, SH 200240, China*

²⁴*Universidad Politécnica de Pachuca, Pachuca, Hgo, Mexico*

²⁵*Department of Physics and Astronomy, University of Utah, Salt Lake City, UT, USA*

²⁶*Instituto de Geofísica, Universidad Nacional Autónoma de México, Ciudad de Mexico, Mexico*

²⁷*University of Seoul, Seoul, Rep. of Korea*

²⁸*Centro de Investigación en Computación, Instituto Politécnico Nacional, México City, México.*

²⁹*Departamento de Física y Matemáticas, Universidad de Monterrey, Monterrey, NL, Mexico*

³⁰*Dept of Physics and Astronomy, University of New Mexico, Albuquerque, NM, USA*

³¹*NASA Goddard Space Flight Center, Greenbelt, MD 20771, USA*

³²*Universidad Autónoma del Estado de Hidalgo, Pachuca, Mexico*

³³*Instituto de Ciencias Nucleares, Universidad Nacional Autónoma de Mexico, Ciudad de Mexico, Mexico*

³⁴*Department of Physics, Missouri University of Science and Technology, Rolla, MO, USA*

³⁵*Department of Physics, Pennsylvania State University, University Park, PA, USA*

(Dated: September 9, 2025)

We conduct an indirect dark matter (DM) search in the Galactic Center, focusing on a square region within $\pm 9^\circ$ in Galactic longitude and latitude, using 2,865 days of data (~ 8 years) from the High-Altitude Water Cherenkov (HAWC) Observatory. We explore DM particles within the Weakly Interacting Massive Particles framework with masses from 1 TeV to 10 PeV. Analyzing three annihilation channels ($b\bar{b}$, $\tau^+\tau^-$, W^+W^-) and three density profiles (Navarro-Frenk-White, Einasto, Burkert), we find no significant excess and set 95% confidence-level upper limits on the velocity-weighted annihilation cross section. Our results provide the first constraints on DM particles well above 100 TeV using gamma-ray data from the Galactic Center, with the strongest limits $\mathcal{O}(10^{-24}) \text{ cm}^3/\text{s}$, from the $\tau^+\tau^-$ channel and the Einasto profile.

Astrophysical and cosmological evidence increasingly suggests that approximately 85% of the Universe's total matter content consists of non-baryonic matter. This matter is commonly referred to as *dark* due to its lack of electromagnetic interaction or luminosity [1–4]. The particle nature of DM remains an open question in modern physics. No suitable candidate exists within the Standard Model (SM). The proposed solutions range from relativistic thermal relic particles to condensates of weakly interacting non-relativistic light bosons [5–8].

One way of probing DM particles is to search for SM particles produced by DM self annihilation. In this work, we focus on the Weakly Interacting Massive Particle (WIMP) scenario, which is accessible to astrophysical observations at the GeV–TeV scale [9, 10]. A particularly compelling aspect of WIMPs is their ability to explain the observed relic abundance of cold DM. If WIMPs were produced in thermal equilibrium in the early Universe and had a weak-scale interaction cross section, they would naturally yield the correct DM density—a phenomenon often referred to as the “WIMP miracle.”

The Galactic Center (GC) is among the most promising targets for indirect DM detection due to the large DM density inferred from astrophysical observations [11]. This region is expected to produce high gamma-ray fluxes from DM annihilation, making it a prime candidate for probing DM signals. Notably, an excess of GeV gamma rays observed by *Fermi*-LAT from the GC has been interpreted as a potential hint of DM annihilation [12–14], though other explanations such as millisecond pulsars also remain viable [14–16]. These results further motivate the need to understand the GC emission at higher energies and testing scenarios of beyond SM physics. Previous searches for WIMP annihilation signatures in the GC and Galactic Halo have set constraints on the velocity-weighted cross section of DM particles with masses below 100 TeV [17–20].

One of the main challenges for searches in this region is the complex astrophysical background, which includes emission from known gamma-ray sources, unresolved sources indistinguishable from the Galactic diffuse emission, and diffuse emission associated with the GC PeVatron [21, 22]. However, instruments with sensitivities

to gamma rays above 100 TeV are particularly powerful, since the Klein–Nishina suppression of inverse Compton scattering reduces leptonic background contributions and enhances sensitivity to potential DM signals [23].

In this *Letter*, we use nearly eight years of data from the High-Altitude Water Cherenkov (HAWC) Gamma-Ray Observatory to search for DM particle masses between 1 TeV and 10 PeV, extending the previously reported range of DM masses [18] and constraining the velocity-weighted cross section of DM particles in the GC with masses well above 100 TeV for the first time. We consider a set of representative annihilation channels ($b\bar{b}$ quarks, $\tau^+\tau^-$ leptons, and W^+W^- bosons) and spatial DM density profiles (Navarro-Frenk-White (NFW), Einasto, and Burkert). We mask known gamma-ray sources to avoid the contamination from their signal. No significant emission is found for any channel or density profile. Therefore, we set 95% confidence-level (CL) upper limits on the velocity-weighted cross section of annihilation. In the following Sections, we describe the HAWC data and our analysis methods, discuss results, and then conclude. Further details are given in the Appendices A–E of the Supplemental Material.

HAWC Data.— The HAWC Observatory, situated at 4,100 m altitude in Parque Nacional Pico de Orizaba, Mexico, detects cosmic and gamma rays with energies between hundreds of GeV and hundreds of TeV by capturing secondary particles produced in atmospheric air showers initiated by astrophysical primaries [24]. Its array of 300 water-Cherenkov detectors operates nearly continuously [25]. The vast majority of showers detected originate from hadronic cosmic rays, creating an isotropic and steady background. Using shower topology cuts [26], we preserve gamma-ray signals while filtering out broader, clumpier hadronic showers. In 2023, the event-reconstruction algorithms were greatly improved (“Pass 5” version), extending the maximum zenith angle to $\sim 56^\circ$, allowing better sensitivity at the edges of HAWC’s field of view [26]. Thanks to these enhancements, HAWC is the only detector capable of observing gamma rays from the GC with energies above 40 TeV [21], allowing us to probe uncharted DM particle masses. Here we use 2,865 days of data and improved reconstruction

algorithms to directly target the region surrounding the GC ($\pm 9^\circ$).

Methods.— For a given DM source and a stable SM particle, the flux of SM particles from DM annihilation into gamma rays (γ) is described as follows:

$$\frac{d\Phi_\gamma}{dE_\gamma} = \frac{\langle\sigma v\rangle}{8\pi M_\chi^2} \frac{dN_\gamma}{dE_\gamma} \times \int_{\text{source}} d\Omega \int_{\text{l.o.s.}} \rho_\chi^2 dl(r, \theta'), \quad (1)$$

where $\langle\sigma v\rangle$ represents the velocity-weighted annihilation cross section of DM to SM particles and M_χ is the DM particle mass. The term $\frac{dN_\gamma}{dE_\gamma}$ denotes the number of photons produced per annihilation. The integral is performed over the solid angle, $d\Omega$, and the line of sight (l.o.s.). The term ρ_χ represents the DM density at a given location, (r, θ') , in the sky.

Various possibilities can be considered for the distribution of DM in the Milky Way. The NFW profile, with a cusp at the GC, is a traditional benchmark from N -body simulations [27]. The Einasto profile is broader at kiloparsec scales and favored by recent simulations [28, 29]. The Burkert profile [30], which features a constant-density core, aligns with observed Galactic rotation curves but is in tension with cold DM-only simulations that predict a steep central cusp. In order to include the spatial signature hypotheses in the likelihood analysis, we calculate the astrophysical component of Equation 1, referred to as the J -factor:

$$J\text{-factor} = \int_{\text{source}} d\Omega \int_{\text{l.o.s.}} \rho_\chi^2 dl(r, \theta'), \quad (2)$$

for each pixel in a map of the region of interest. These J -factor spatial distributions are produced using `Gammapy` [31]—an open-source Python package for gamma-ray astronomy. More details can be found in Appendix A.

The spectral models implemented in this analysis are imported from `HDMSpectra` [32], which provides the expected photon spectra for DM annihilation to different SM channels, constituting a wide variety of hypotheses. These annihilation spectra assume prompt emission, neglecting any subsequent propagation or energy loss effects [33]. Gamma rays with TeV energies also undergo attenuation by interaction with the cosmic microwave background and other galactic radiation fields [34]. This effect would be most relevant for the highest DM masses considered in this analysis. However, we note that even for PeV DM, HAWC’s sensitivity comes from being able to probe the tail of the DM spectrum that extends below 200 TeV. At these energies, the expected attenuation from distance to the GC is $\sim 20\%$ [35]. The impact is subdominant compared to the other systematic uncertainties in this analysis such as the DM profile and detector systematics. The Test Statistic (TS) is computed with the log-likelihood ratio test, which compares the

expected number of events from DM annihilation to the background-only hypothesis. The best-fit signal parameters correspond to the value of $\langle\sigma v\rangle$ (Equation 1) that maximizes the likelihood.

In Figure 1, we show the significance map of the $\pm 9^\circ$ region around the GC, where the analysis is conducted. The blank region in the bottom right corresponds to zenith angles beyond $\sim 56^\circ$, where HAWC’s reconstruction and simulations are not optimized. This region is therefore excluded from the analysis.

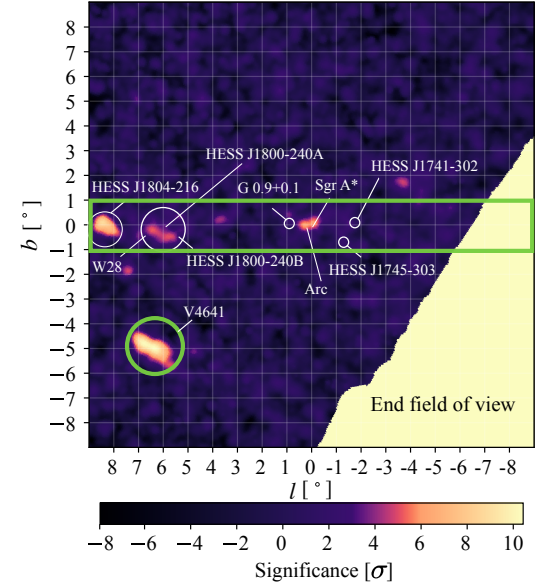


FIG. 1. Significance map of the region of interest used for this analysis. The significance is defined as $\sqrt{\text{TS}}$. The labels indicate very-high-energy gamma-ray sources. The green rectangle and circle outline the masks. The bottom right region is the end of HAWC’s field of view ($\sim 56^\circ$ zenith angle) and is excluded from the likelihood fit. Color available online.

To mitigate contamination from known gamma-ray sources, we mask them in the HAWC data by setting the J -factor in the corresponding pixels to zero. The Galactic Plane is masked with a $\pm 1^\circ$ band, effectively removing sources with spectral index < 2.5 or coincident with $> 3\sigma$ hotspots. The only known source outside this band, V4641 Sagittarius [36], is masked separately. The size of these masks are conservative, with sizes larger than HAWC’s angular resolution at this declination.

Results.— No significant excess was found in the probed mass range (1 TeV–10 PeV). Therefore, upper limits on $\langle\sigma v\rangle$ were placed at the 95% CL (see details in Appendix B). In Figure 2, we show the upper limit on $\langle\sigma v\rangle$ at the 95% CL for the three channels assuming the Einasto density profile. The mean expected upper

limit is also shown along with the 68% and 95% containment bands, which are obtained from 300 Poisson realizations of the background (more details in Appendix C). In all three cases, the limits deviate from expectations only within the 95% confidence band. This suggests that the deviations are driven purely by Poisson fluctuations rather than an unaccounted source or a mischaracterization of the background. The $\tau^+\tau^-$ channel yields the strongest limits due to its hard gamma-ray spectrum, to which HAWC is more sensitive. Detector systematic uncertainties in HAWC are evaluated by performing the analysis with modified detector response functions. In all cases, the resulting uncertainties are found to be below 30% (more details in Appendix D).

In Figure 3, we compare our limits with previous results from HAWC, the High-Energy Stereoscopic System (H.E.S.S.), and IceCube. Compared to HAWC’s 2023 Galactic Halo analysis [18], we extend the mass range by a factor of four using more data and improved reconstruction. Our limits are up to twice as strong between 10–100 TeV for $b\bar{b}$ and $\tau^+\tau^-$ and are comparable for W^+W^- .

H.E.S.S. has greater sensitivity below 70 TeV due to its finer angular resolution and optimal location in the Southern Hemisphere, while HAWC—observing the GC at high zenith—probes higher masses, beyond H.E.S.S.’s reach. IceCube’s Galactic Center limits are stronger below 7 TeV, but our limits become comparable or stronger above that, particularly for $b\bar{b}$. An equivalent figure using the Burkert profile can be found in Appendix E of the Supplemental Material.

Summary.— In this *Letter*, we present an indirect DM search in the GC using nearly eight years of HAWC data, probing WIMP annihilation in the 1 TeV–10 PeV mass range. We masked the Galactic Plane and other known sources to mitigate gamma-ray contamination. The lack of a significant excess in all density profiles and channels probed allows us to place 95% CL constraints on the velocity-weighted annihilation cross section of WIMPs.

These results provide the first gamma-ray constraints above 100 TeV from the GC. The strongest limits are found for the $\tau^+\tau^-$ channel assuming an Einasto profile. While the maximum mass of thermal freeze-out WIMPs is subject to the unitarity bound of about 130 TeV, our results are applicable to various models that predict non-thermal mechanisms of DM production in which the masses can be as high as 10^6 TeV [37, 38]. Although H.E.S.S. is more sensitive at lower energies, HAWC uniquely probes the multi-TeV to PeV mass range. Compared to IceCube and prior HAWC results, our limits improve significantly above 10 TeV. Systematic uncertainties remain below 30% for all profiles and channels. While uncertainties related to the J -factor and radiative corrections to the channel spectra are not explicitly included, the differences between the assumed den-

sity profiles encompass the dominant uncertainties in the DM distribution [39].

This study extends the experimental frontier of indirect DM detection to PeV-scale masses and strengthens constraints on particle annihilation in one of the most promising regions for DM concentration. Our results help narrow the parameter space of heavy thermal relics, while providing valuable input for both particle theory and GC astrophysics. Future work including analysis of data from next-generation Southern Hemisphere observatories such as the Cherenkov Telescope Array and the Southern Wide-field Gamma-Ray Observatory will further extend the reach of gamma-ray searches.

Acknowledgments.— We acknowledge the support from: the US National Science Foundation (NSF); the US Department of Energy Office of High-Energy Physics; the Laboratory Directed Research and Development (LDRD) program of Los Alamos National Laboratory; Consejo Nacional de Ciencia y Tecnología (CONACYT), México, grants LNC-2023-117, 271051, 232656, 260378, 179588, 254964, 258865, 243290, 132197, A1-S-46288, A1-S-22784, CF-2023-I-645, cátedras 873, 1563, 341, 323, Red HAWC, México; DGAPA-UNAM grants IG101323, IN111716-3, IN111419, IA102019, IN106521, IN114924, IN110521, IN102223; VIEP-BUAP; PIFI 2012, 2013, PROFOCIE 2014, 2015; the University of Wisconsin Alumni Research Foundation; the Institute of Geophysics, Planetary Physics, and Signatures at Los Alamos National Laboratory; Polish Science Centre grant, 2024/53/B/ST9/02671; Coordinación de la Investigación Científica de la Universidad Michoacana; Royal Society - Newton Advanced Fellowship 180385; Gobierno de España and European Union-NextGenerationEU, grant CNS2023- 144099; The Program Management Unit for Human Resources & Institutional Development, Research and Innovation, NXPO (grant number B16F630069); Coordinación General Académica e Innovación (CGAI-UdeG), PRODEP-SEP UDG-CA-499; Institute of Cosmic Ray Research (ICRR), University of Tokyo. H.F. acknowledges support by NASA under award number 80GSFC21M0002. C.R. acknowledges support from National Research Foundation of Korea (RS-2023-00280210). We also acknowledge the significant contributions over many years of Stefan Westerhoff, Gaurang Yodh and Arnulfo Zepeda Domínguez, all deceased members of the HAWC collaboration. Thanks to Scott Delay, Luciano Díaz and Eduardo Murrieta for technical support.

[1] J. L. Feng, *Ann. Rev. Astron. Astrophys.* **48**, 495 (2010), [arXiv:1003.0904 \[astro-ph.CO\]](https://arxiv.org/abs/1003.0904).

[2] M. R. Buckley and A. H. G. Peter, *Phys. Rept.* **761**, 1 (2018), [arXiv:1712.06615 \[astro-ph.CO\]](https://arxiv.org/abs/1712.06615).

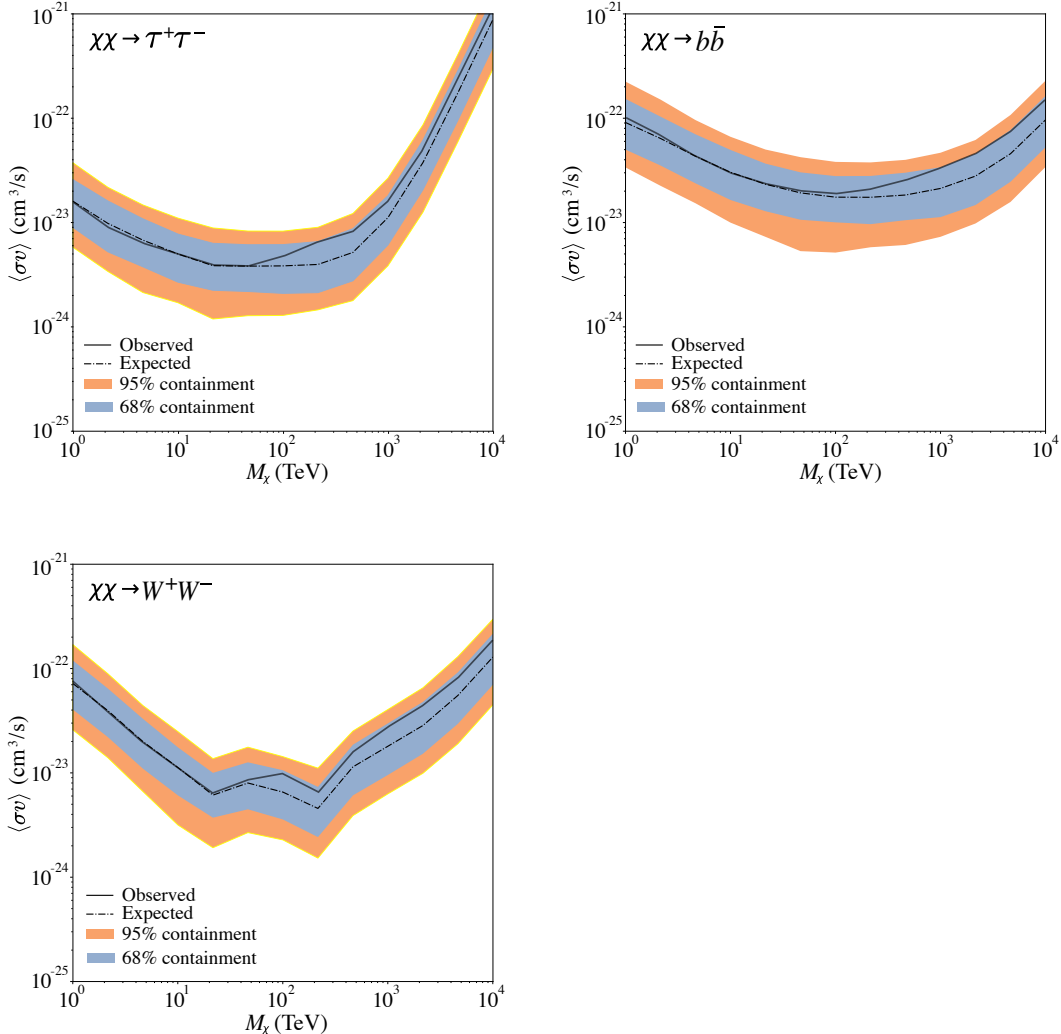


FIG. 2. Containment bands for the 1 and 2σ expected limits compared to the observed upper limit at the 95% CL, assuming an Einasto density profile for the channels: **upper left** $\tau^+\tau^-$, **upper right** $b\bar{b}$, and **bottom left** W^+W^- .

- [3] C. Patrignani, *Chinese Physics C* **40**, 100001 (2016).
- [4] K. Freese, *Int. J. Mod. Phys. A* **1**, 325 (2017), [arXiv:1701.01840 \[astro-ph.CO\]](https://arxiv.org/abs/1701.01840).
- [5] L. D. Duffy and K. van Bibber, *New Journal of Physics* **11**, 105008 (2009).
- [6] D. Antypas, A. Banerjee, C. Bartram, M. Baryakhtar, J. Betz, J. Bollinger, C. Boutan, D. Bowring, D. Budker, D. Carney, *et al.*, arXiv preprint arXiv:2203.14915 (2022).
- [7] T. Hambye, M. H. G. Tytgat, J. Vandecasteele, and L. Vanderheyden, *Phys. Rev. D* **100**, 095018 (2019).
- [8] A. Kusenko, *Physics Reports* **481**, 1 (2009).
- [9] G. Bertone, *Particle dark matter: observations, models and searches* (Cambridge University Press, 2010).
- [10] J. L. Feng, *Annual Review of Astronomy and Astrophysics* **48**, 495 (2010).
- [11] A. Cesarini, F. Fucito, A. Lionetto, A. Morselli, and P. Ullio, *Astroparticle Physics* **21**, 267 (2004).
- [12] T. Daylan, D. P. Finkbeiner, D. Hooper, T. Linden, S. K. Portillo, N. L. Rodd, and T. R. Slatyer, *Physics of the Dark Universe* **12**, 1 (2016).
- [13] R. K. Leane and T. R. Slatyer, *Phys. Rev. Lett.* **123**, 241101 (2019).
- [14] S. Murgia, *Annual Review of Nuclear and Particle Science* **70**, 455 (2020).
- [15] R. Bartels, S. Krishnamurthy, and C. Weniger, *Phys. Rev. Lett.* **116**, 051102 (2016).
- [16] R. Bartels, E. Storm, C. Weniger, and F. Calore, *Nature Astronomy* **2**, 819 (2018).
- [17] H. Abdalla, F. Aharonian, F. A. Benkhali, E. Angüner, C. Armand, H. Ashkar, M. Backes, V. Baghmanyan, V. B. Martins, R. Batzofin, *et al.*, *Physical Review Letters* **129**, 111101 (2022).
- [18] A. Albert, R. Alfaro, C. Alvarez, J. Arteaga-Velázquez, D. A. Rojas, H. A. Solares, E. Belmont-Moreno, K. Caballero-Mora, T. Capistrán, A. Carramiñana, *et al.*, *Journal of Cosmology and Astroparticle Physics* **2023**, 038 (2023).

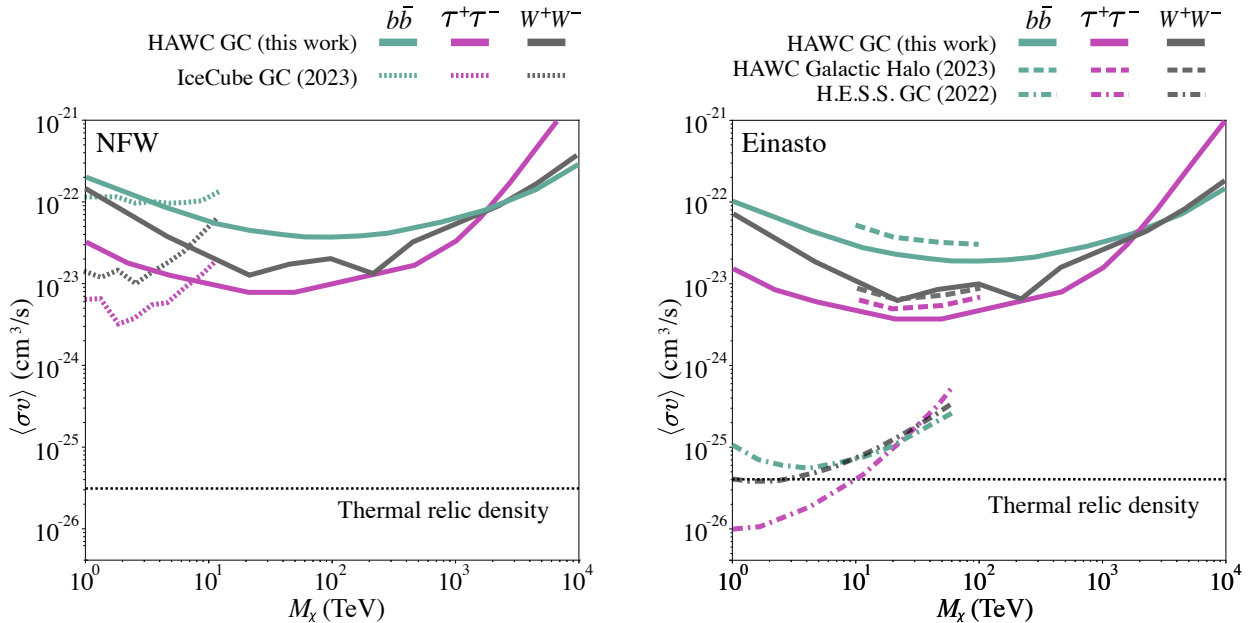


FIG. 3. Upper limits at 95% CL on the velocity-weighted annihilation cross section for the channels: $b\bar{b}$ (cyan), $\tau^+\tau^-$ (purple), and W^+W^- (black) assuming the **left** NFW density profile compared to IceCube [19] (dotted lines) and the **right** Einasto density profile compared to HAWC (“Pass 4” version; dashed lines) [18] and H.E.S.S. [17] (dash-dotted lines). The regions above the curves are excluded. Color version online

- [19] R. Abbasi, M. Ackermann, J. Adams, S. K. Agarwalla, J. A. Aguilar, M. Ahlers, Alameddine, *et al.* (IceCube Collaboration), *Phys. Rev. D* **108**, 102004 (2023).
- [20] K. N. Abazajian, S. Horiuchi, M. Kaplinghat, R. E. Keeley, and O. Macias, *Physical Review D* **102**, 043012 (2020).
- [21] A. Albert, R. Alfaro, C. Alvarez, A. Andrés, J. C. Arteaga-Velázquez, D. A. Rojas, H. A. A. Solares, *et al.*, *The Astrophysical Journal Letters* **973**, L34 (2024).
- [22] H. Collaboration, *Nature* **531**, 476 (2016).
- [23] O. Klein and Y. Nishina, *Nature* **122**, 398 (1928).
- [24] A. U. Abeysekara, A. Albert, R. Alfaro, C. Alvarez, J. D. Álvarez, R. Arceo, *et al.*, *Astrophys. J.* **843**, 39 (2017), [arXiv:1701.01778 \[astro-ph.HE\]](https://arxiv.org/abs/1701.01778).
- [25] A. Abeysekara, A. Albert, R. Alfaro, C. Alvarez, J. Álvarez, M. Araya, J. Arteaga-Velázquez, K. Arunbabu, *et al.*, *Nuclear Instruments and Methods in Physics Research Section A: Accelerators, Spectrometers, Detectors and Associated Equipment* **1052**, 168253 (2023).
- [26] A. Albert, R. Alfaro, C. Alvarez, A. Andrés, J. C. Arteaga-Velázquez, D. A. Rojas, H. A. A. Solares, R. Babu, E. Belmont-Moreno, A. Bernal, K. S. Caballero-Mora, *et al.*, *The Astrophysical Journal* **972**, 144 (2024).
- [27] J. F. Navarro, C. S. Frenk, and S. D. M. White, *ApJ* **462**, 563 (1996), [arXiv:astro-ph/9508025 \[astro-ph\]](https://arxiv.org/abs/astro-ph/9508025).
- [28] D. Merritt, A. W. Graham, B. Moore, J. Diemand, and B. Terzić, *The Astronomical Journal* **132**, 2685 (2006).
- [29] J. F. Navarro, A. Ludlow, V. Springel, J. Wang, M. Vogelsberger, S. D. M. White, A. Jenkins, C. S. Frenk, and A. Helmi, *Monthly Notices of the Royal Astronomical Society* **402**, 21 (2010), <https://academic.oup.com/mnras/article-pdf/402/1/21/18573804/mnras0402-0021.pdf>.
- [30] A. Burkert, *The Astrophysical Journal* **447**, L25 (1995).
- [31] A. Donath, R. Terrier, Q. Remy, A. Sinha, C. Nigro, *et al.*, *Astronomy & Astrophysics* **678**, A157 (2023).
- [32] C. W. Bauer, N. L. Rodd, and B. R. Webber, *Journal of High Energy Physics* **2021** (2021), [10.1007/jhep06\(2021\)121](https://doi.org/10.1007/jhep06(2021)121).
- [33] T. R. Slatyer, *SciPost Phys. Lect. Notes* , 53 (2022).
- [34] A. Esmaili and P. D. Serpico, *JCAP* **2015**, 014 (2015), [arXiv:1505.06486 \[hep-ph\]](https://arxiv.org/abs/1505.06486).
- [35] J. Zhang and Y. Guo, [arXiv:2409.00477](https://arxiv.org/abs/2409.00477) (2024), [arXiv:2409.00477 \[astro-ph.HE\]](https://arxiv.org/abs/2409.00477).
- [36] R. Alfaro, C. Alvarez, *et al.*, *Nature* **634**, 557 (2024).
- [37] E. D. Kramer, E. Kuflik, N. Levi, N. J. Outmezguine, and J. T. Ruderman, *Phys. Rev. Lett.* **126**, 081802 (2021), [arXiv:2003.04900 \[hep-ph\]](https://arxiv.org/abs/2003.04900).
- [38] N. Bernal, P. Konar, and S. Show, *Phys. Rev. D* **109**, 035018 (2024).
- [39] M. Cirelli, P. Panci, and G. Servant, *JCAP* **03**, 051 (2011), [arXiv:1012.4515 \[hep-ph\]](https://arxiv.org/abs/1012.4515).
- [40] L. Posti and A. Helmi, *Astronomy & Astrophysics* **621**, A56 (2019).
- [41] F. Iocco, M. Pato, and G. Bertone, *Nature Physics* **11**, 245 (2015).
- [42] G. Cowan, K. Cranmer, E. Gross, and O. Vitells, *The European Physical Journal C* **71**, 1554 (2011).

Supplemental Material for

Search for Signatures of Dark Matter Annihilation in the Galactic Center with HAWC

HAWC Collaboration

We provide additional details in the appendices below to aid the reading of the paper. Appendix A gives details regarding the density profiles and J -factor computation. Appendices B and C describe how the upper and expected limits were computed. Appendix D gives details about the calculation of systematic uncertainties. Finally, Appendix E shows the limits for the Burkert density profile.

Appendix A: Density profiles for the Galactic Center and J -factor computation in the regions of interest

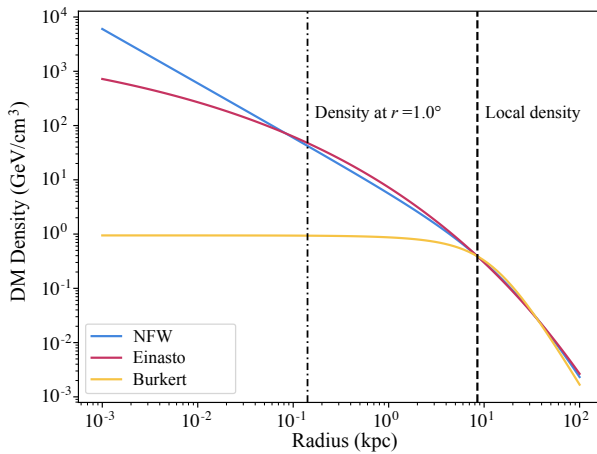
Various possibilities can be considered for the distribution of DM in the Milky Way. In particular, this work considers the NFW, Einasto, and Burkert density profiles, which are shown in Supplemental Figure 1. Given the lack of consensus on the true DM profile, exploring the full range of these models is essential for robust predictions of DM signals in the Milky Way. The functional forms of these profiles are given by:

$$\rho_{\text{NFW}}(r) = \rho_s \frac{r_s}{r} \left(1 + \frac{r}{r_s}\right)^{-2}, \quad (\text{S1})$$

$$\rho_{\text{Ein}}(r) = \rho_s \exp \left[-\frac{2}{\alpha} \left(\frac{r}{r_s} \right)^\alpha - 1 \right], \quad (\text{S2})$$

$$\rho_{\text{Bur}}(r) = \frac{\rho_s}{(1 + r/r_s)(1 + (r/r_s)^2)}, \quad (\text{S3})$$

where $\rho_s = 0.39 \text{ GeV/cm}^3$ is the local density, $\alpha = 0.17$ is an empirical fit to numerical simulations of DM halos, and $r_s = 20 \text{ kpc}$ is a scale value based on theoretical models and observational constraints [40, 41].



SUPPL. FIG. 1. The three DM density profiles considered in this analysis: NFW (blue), Einasto (red), and Burkert (yellow). It is worth noting that the Burkert profile features a significantly more flat, low-density center (“cored”) DM distribution, resulting in lower central densities at the GC compared to the cusped NFW and Einasto profiles. The dash-dotted line marks the distance equivalent to the width of the Galactic plane mask (1.0°). The dashed line shows the distance from Earth to the GC.

Appendix B: Computation of upper limits

The TS is computed with the log-likelihood ratio test:

$$TS = -2 \ln \left(\frac{L_{\text{null}}}{L_{\text{model}}} \right), \quad (\text{S4})$$

where L_{model} is the likelihood of the model with a DM annihilation source and L_{null} is the likelihood of the background-only alternative. The best-fit signal parameters are found where $\langle \sigma v \rangle$ in Equation 1 maximizes the likelihood.

To determine the upper limit at the 96% CL, we began by calculating the TS for $\langle \sigma v \rangle$. The value of $\langle \sigma v \rangle$ that yielded the largest TS value from Equation S4, TS_{max} , was then determined by scanning over increasing values of $\langle \sigma v \rangle$. To find the 96% CL limit, we scan $\langle \sigma v \rangle$ until the TS decreases by $\Delta TS = 2.71$, which is determined from the appropriate distribution for a non-negative signal parameter [42] and satisfies:

$$\frac{1}{2} + \frac{1}{2} F_{\chi^2}(\Delta TS) = 0.95, \quad (\text{S5})$$

where F_{χ^2} is the cumulative distribution function of a χ^2 distribution with 1 degree of freedom.

The upper limit on the velocity-weighted cross section, $\langle \sigma v \rangle_{95}$, is then defined as the value for which

$$TS(\langle \sigma v \rangle_{95}) = TS_{\text{max}} - \Delta TS.$$

This procedure is repeated for each DM density profile and annihilation channel to obtain the 95% CL upper limits.

Appendix C: Computation of expected limits and exclusion bands

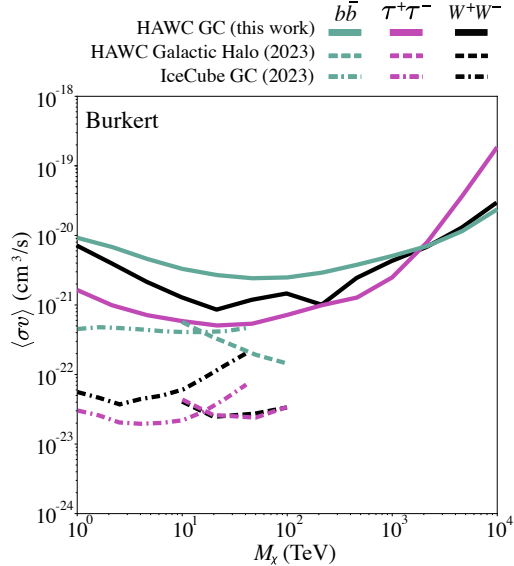
To compute the effects of statistical fluctuations on the limits, we calculate the 68% and 95% containment bands, which are produced from 300 Poisson realizations of the null hypothesis (background only). These Poisson realizations are pseudomaps where the data in each bin are replaced with a randomly drawn value from a Poisson distribution with a mean equal to the estimated background in that bin. The median of the resulting distribution produces the expected limits assuming the null hypothesis of a background-only model is true.

Appendix D: Systematic uncertainties

Since we are studying the same region as in Reference 21, we selected the two configurations of the detector that resulted in the largest systematic uncertainty in that analysis, late-light simulation and absolute PMT efficiency comparing different epochs in time, which are described in Reference 26. The systematic uncertainties are <30% for all three density profiles.

Appendix E: Burkert profile

The upper limits derived using the Burkert profile are shown in Supplemental Figure 2. These are approximately two orders of magnitude weaker than those obtained assuming the Einasto and NFW profiles. The absence of a central cusp results in a lower predicted gamma-ray flux, necessitating a larger region of interest to capture comparable emission. However, in this study we maintained a consistent region of interest across different profiles restricting the detectable flux, thereby reducing sensitivity and weakening the constraints relative to the cuspy NFW and Einasto profiles. The same argument can be used to explain the difference between our limits and the ones obtained by HAWC targeting the Galactic Halo instead.



SUPPL. FIG. 2. Upper limits at 95% CL on the velocity-weighted annihilation cross section for the channels: $b\bar{b}$ (cyan), $\tau^+\tau^-$ (purple), and W^+W^- (black) assuming the Burkert profile compared to HAWC (“Pass 4” version; dashed lines) [18] and IceCube [19] (dotted lines). Note that the y -axis is different from the one in Figure 3. Color available online.